Roman Letters

# Simplified Iterative Maneuver Optimization in a Transverse Gust Encounter

Xianzhang Xu\* and Francis D. Lagor<sup>†</sup> *University at Buffalo, The State University of New York, Buffalo NY 14260* 

Wing-gust encounters cause harmful lift transients that can be mitigated through maneuvering of the wing. This paper presents a method to generate an open-loop (i.e., prescribed) maneuver that optimally regulates the lift on the wing during a transverse gust encounter. Obtaining an optimal maneuver is important for laboratory experiments on the physics of wing-gust interactions and may be useful for the future design of feedback controllers. Prior work of the authors has shown that an Iterative Maneuver Optimization (IMO) framework can generate an optimal maneuver by using a surrogate model to propose a control signal that is then tested in experiment or high-fidelity simulation. The input to the surrogate model is updated to account for differences between the test data and the expected output. The optimal maneuver is obtained through iteration of this process. This paper simplifies the IMO method by replacing the surrogate model with the classical lift model of Theodorsen, removing the process of optimization over the surrogate model, and removing the requirement to know the time-averaged profile of the gust. The proposed method, referred to as Simplified IMO (SIMO), only requires input and output data collected from simulations or experiments that interact with the gust. Numerical simulations using a Leading Edge Suction Parameter modulated Discrete Vortex Model (LDVM) are presented to generate the input and output data of the wing-gust encounters for this paper. The results show an optimal pitch maneuver and an optimal plunge maneuver that can each regulate lift during a transverse gust encounter.

# I. Nomenclature

pitch axis location in semi-chords Fourier coefficients  $A_0, A_n$ semi-chord length, c/2h chord length lift coefficient, drag coefficient  $C_L, C_D$ suction force coefficient, normal force coefficient  $C_S, C_N$ reference value for lift coefficient  $C_{L,\mathrm{ref}}$ lift coefficient predicted by the surrogate model  $C_{L, \text{model}}$ lift coefficient measured in experiment or high-fidelity simulation  $C_{L,\text{test}}$ GR gust ratio,  $V_{\rm max}/\overline{V}$  $h, \dot{h}, \ddot{h}$ plunge amplitude, plunge rate, plunge acceleration performance measure for optimal control  $K_p, K_i, K_d$ proportional, integral, derivative control gain reduced frequency of the wing motion LESPc critical value of Leading Edge Suction Parameters pressure p Ġ surge rate convective time, Ut/cstart time and terminal times of the optimal control problem  $t_0, t_f$ external flow components in the inertial reference frame  $(u_x, u_z)$ 

<sup>\*</sup>Graduate Student, Department of Mechanical and Aerospace Engineering, AIAA Student Member

<sup>†</sup>Assistant Professor, Department of Mechanical and Aerospace Engineering, AIAA Senior Member

 $U_{\text{ref}}$  = constant, characteristic flow speed U = relative flow speed, freestream flow  $(u_{\text{ind}}, w_{\text{ind}})$  = components of induced flow velocity  $V_{\text{max}}$  = maximum velocity of gust flow model

W = gust widthW = downwash

x = location along the chord line

 $(x_C, z_C)$  = coordinates of pitch axis in the body frame of the wing

y = output signals

### Greek Letters

 $\alpha, \dot{\alpha}, \ddot{\alpha}$  = angle of attack, angle-of-attack rate, angle-of-attack acceleration

 $\gamma$  = strength of bound-vortex sheet  $\Gamma$  = circulation strength of discrete vortex  $\theta, \dot{\theta}, \ddot{\theta}$  = pitch angle, pitch rate, pitch acceleration  $\nu$  = angular coordinate along chord line

# **II. Introduction**

Gust encounters can de-stabilize the flight of small, unmanned aerial vehicles and lead to significant damage [1, 2]. GConsequently, wing motions and wing-gust encounters have been studied with great interest at low Reynolds numbers (e.g., see [3–5]). Existing atmospheric flight controllers perform model-based control in unsteady flow environments by treating the gust as a disturbance input that can be rejected through linear robust control techniques [6–8]. However, these vehicles often encounter transverse gusts that can produce large disturbances and induce shedding of coherent flow structures that greatly influence the aerodynamic forces [9, 10]. Hence, more recent studies have investigated the structure of the flow field during transverse wing-gust encounters at low Reynolds numbers in both high-fidelity numerical simulations [11, 12] and experiments [13]. Findings indicate that large-amplitude transverse gusts can cause massive flow separation, resulting in deviation of the lift force from its steady value prior to the encounter. Often, a large lift overshoot occurs early in the encounter, and a lift deficit can occur while exiting the gust. Many attempts to mitigate the effects of the gust have focused on maneuvering the wing [14–16]. Maneuvering the wing can influence the circulatory, non-circulatory, and added-mass contributions to the lift force by altering the wing's orientation and rates of change during the encounter [4]. Sedky [17] has shown that pitch maneuvers can regulate lift near either zero or non-zero values.

Minimizing absolute deviations of the lift from a reference value is a regulation problem in the study of control. There are many modern control techniques to address regulation problems for linear and nonlinear systems. However, many of these tools are model-based and would require modeling and identification (i.e., quantifying parameters) of the wing-gust system prior to use. Poor modeling or system identification can lead to poor performance of the controller, and even instability of the closed-loop system. Proportional-Integral-Derivative (PID) controllers can often work for control problems in which the system model is uncertain or unknown. However, to obtain performance guarantees for a PID controller requires a system model for closed-loop analysis.

In wing-gust encounters, the fluid system has unsteady, nonlinear, and multi-scale dynamics, which makes capturing all relevant physical effects difficult. Recent works in gust-encounter research have sought low-order models for the wing-gust interaction for the purposes of interpreting experimental data through the lens of the model [4], designing feedback controllers [15], and designing prescribed maneuvers [16, 18]. Early potential-flow models of wing-gust encounters developed by Wagner, Theodorsen, Küssner, and von Kármán [19–22] have been examined for applicability to large-amplitude gusts. Andreu-Angulo et al. [14] combined different classic aerodynamic theories to model the effects of gust flow and wing kinematics. They used their model to design a maneuver that maintains a specified effective angle of attack during the encounter. These models provide some useful, predictive capability, despite assumptions of low-frequency motion and attached flow.

To include external vorticity in a potential-flow model, Corkery et al. [23] modeled the shear layers of a transverse gust using discretized vortex sheets to study the forces on the wing. Since shed vorticity, such as the Leading Edge Vortex (LEV) can greatly impact the lift force [24, 25], some studies simulate wing-gust encounters using a Discrete Vortex Model (DVM) in which vortices freely advect within a potential flow model. Andreu-Angulo and Babinsky [18] used a DVM to design a prescribed maneuver by pitching the wing to zero out the lift calculated within the model at each

time step. Sedky et al. [18, 26] used a DVM to assess the performance of a proportional feedback controller that was tuned using Theodorsen's unsteady aerodynamic model. In prior work [16], the authors designed an optimal pitching maneuver for a nonlinear, modified Goman-Khrabrov (mGK) model [27] of a gust encounter using an optimal-control framework based on a gradient-descent approach. These works demonstrate lift regulation with appropriate wing maneuvers, however, lift forces still experience deviations from the desired reference value when the profile is applied in experiment or high-fidelity simulation. These deviations are attributable to unmodeled effects, because the prescribed profile or feedback controller is subject to the limitations of the model used in its construction.

To study mechanisms of force mitigation through wing maneuvering, it is desirable to use a motion profile that is truly optimal, or at least as nearly optimal as possible. An optimal maneuver may provide valuable insight into wing-gust interaction that may inform future design of feedback controllers. Hence, the goal of this paper is to create a reliable method for off-line calculation of open-loop optimal maneuvers that can be utilized in experimental and computational research. In addition, we seek to reduce dependence on the model used during maneuver construction. One way to accomplish this goal is by incorporating experimental or high-fidelity simulation data from the system under study during maneuver construction.

Data-driven methods, such as Proper Orthogonal Decomposition (POD) [28] and Dynamic Mode Decomposition (DMD) [29], have become important tools for the analysis and reduced-order modeling of fluid systems [30]. These algorithms can provide an accurate, linear representation of the system. Extensions of the DMD algorithm have also addressed nonlinearities [31] and can include control inputs [32]. Unfortunately, identified linear control models are only valid at (or very close to) the prescribed inputs used in model construction. Changes in actuation require changes in the system model, which makes use of these approaches in optimal control calculations difficult. Deem et al. [33] used an adaptive LQR controller with the online DMD algorithm that updates the system model as new data arrives. Deem et al. [33] note that the control input is not optimal due to non-linearity and time-varying features of the fluid system. Addressing the time-varying nature of a fluid system in construction of an optimal control signal may be possible if the flow is highly repeatable in experiment or simulation.

Rather than online construction of an optimal control, repeated experiments or simulations can provide data for offline refinement of the control. Some data-driven control methods tune the control signal in an iterative manner, such as Iterative Tuning Feedback (IFT) [34] and Iterative Learning Control (ILC) [35]. These methods use the error between the output signal and a desired output signal to update the control design or a reference signal for the controller in the next iteration. An iteration in either of these methods consists of applying the updated controller or control signal in experiment or high-fidelity simulation. IFT uses the output error information to adjust controller gains, while ILC uses the output error to adjust a reference input signal. In the authors' prior work [36], a method similar to ILC, called Iterative Maneuver Optimization (IMO), is applied to generate optimal maneuvers of a wing in a gust encounter through iterated experiments. The fundamental principle behind IMO is the same as ILC. However, the methods differ, because ILC typically applies to linear systems and uses a learning filter for the signal update, while IMO performs control signal updates by solving an optimal control calculation using a surrogate model.

The IMO method uses an optimal control calculation on an mGK model and several iterations through experiment or higher-fidelity simulation to generate an optimal maneuver for the true wing-gust system. In [36], the authors show that the mGK model produces an undesirable delay in the lift response during a gust encounter. However, the IMO method is able to overcome this deficiency to produce an optimal maneuver in simulation and a highly optimized maneuver in experiment. Although the IMO method is very useful, it has several limitations. In particular, the IMO method requires prior knowledge of the gust profile to derive the optimal control input using the mGK model. The mGK model also contains empirical terms that must be fit using initial experiments. Lastly, the optimal control procedure is slow and complex. The main objective of this paper is to simplify the IMO method.

This paper creates an iterative procedure that the authors refer to as Simplified IMO (SIMO). SIMO uses the classic unsteady lift model of Theodorsen [19] to predict the lift from the wing's maneuvers. Theodorsen's lift model includes pitching and plunging effects, as well as a term that accounts for wake vorticity. Brunton et al. [37] previously designed a controller by taking the Laplace transformation of Theodorsen's function to obtain transfer functions from the maneuver inputs to lift. Sedky et al. [26] considered the transverse gust as an output disturbance and designed an output feedback controller based on robustness arguments and the sensitivity transfer function. This approach successfully removes the requirement for prior knowledge of the gust profile, but it still requires an anticipated reduced frequency range for the gust disturbance. In this paper, the SIMO method utilizes Theodorsen's lift model to replace the mGK surrogate model in IMO and designs output feedback controllers for Theodorsen's pitch and plunge models to track a reference lift signal. The optimal maneuvers that regulate the lift of the wing during the transverse gust encounter are generated through an iterative approach and do not require any prior knowledge of the gust. Pitch acceleration and plunge acceleration inputs

are studied individually using a DVM simulation with leading edge shedding modulated by the Leading Edge Suction Parameter (LESP) as the test system. This form of DVM is referred to in this paper as an LDVM.

The contributions of this paper are: 1) a method to construct an optimal lift-regulating maneuver in a transverse gust encounter based on Theodorsen's unsteady lift model and iterated experimentation, and 2) determination of an optimal lift-regulating maneuver using only a plunge input in numerical experiment with an LDVM simulation. These contributions are important because the simplified method for maneuver optimization greatly reduces the experimentation effort required by removing the need to initially characterize the wing and the gust (i.e., empirically determine coefficients and the time-averaged gust profile). Additionally, examination of a plunge input expands on the previous work of the authors that only examined a pitching input in the IMO process.

This paper is organized as follows: Section III reviews the LDVM modeling technique for simulation of wing-gust encounters. Section IV reviews the IMO method for determining an optimal maneuver for force regulation. Section V presents the framework of the Simplified IMO method and its application to design pitch or plunge maneuvers for lift regulation. Section VI presents simulation results and discusses the relative merits and disadvantages of the SIMO method. Section VII concludes the paper and discusses future work.

# III. Discrete Vortex Model of Wing-Gust Encounters

This section reviews the Discrete Vortex Model with Leading Edge Suction Parameter (LDVM), which is used in numerical experiments in this work.

#### A. Discrete Vortex Model Formulation

DVMs have been extensively used in modeling unsteady aerodynamic phenomena, such as formation and shedding of the Leading Edge Vortex (LEV) [25, 38, 39]. DVM methods are able to produce flow fields that closely agree with CFD and experiments for fluid problems, such as LEV formation, dynamic stall, and high angle-of-attack motion [25, 38–40]. Recent research [26, 41] has employed DVM methods to model fluid dynamic problems with external flow disturbances. SureshBabu et al. [41] investigate a maneuvering airfoil encountering a flow disturbance generated by an upstream cylinder through numerical simulation with a DVM model. DVM methods have also been utilized to model wing-gust encounters. As discussed by [26], a gust can be modeled using a prescribed velocity field that does not deform according to the wing's motion, or can be modeled using free vortices initially aligned in the shape of the gust that subsequently deform with the wing's motion. For the gust studied in [26], only minor differences in the lift prediction were noticed between these two approaches, but the prescribed velocity field approach provided significant computational savings. A DVM is selected to model the gust encounter, because it is able to represent shedding of vorticity in response to a prescribed velocity field of the gust. The non-dimensional LESP quantity introduced by Ramesh et al. [25] serves as the criterion of leading-edge shedding. When the LESP value exceeds the critical value, LESPc, which is determined empirically from experimental or CFD data, the airfoil sheds vortices from the leading edge. The trailing edge of the airfoil continuously sheds vortices. This method was built on the time-stepping approach introduced by Katz and Plotkin [24].

In thin-airfoil theory, a bound vortex distribution within the airfoil enforces a boundary condition of no flow through the airfoil. The sheet strength, at time t, is given by the Fourier series [41]

$$\gamma(\nu, t) = 2U_{\text{ref}} \left[ A_0(t) \frac{1 + \cos \nu}{\sin \nu} + \sum_{n=1}^{\infty} A_n(t) \sin(n\nu) \right]$$
 (1)

Here,  $U_{\text{ref}}$  is a non-dimensional characteristic speed associated with the problem, and  $\nu$  is an angular coordinate that is associated with the chordwise coordinate x through the Glauert transformation,  $x = c(1 - \cos \nu)/2$ . The time-dependent Fourier coefficients [41]

$$A_0(t) = -\frac{1}{\pi} \int_0^{\pi} \frac{W(v, t)}{U_{\text{ref}}} dv$$

$$A_n(t) = \frac{2}{\pi} \int_0^{\pi} \frac{W(v, t)}{U_{\text{ref}}} \cos(nv) dv,$$
(2)

are calculated using the downwash W(v,t), which is the velocity impinging on the airfoil normal to the chord line. The downwash is calculated from the velocity induced by the kinematics of the airfoil, discrete vortices in the flow field, and external flow due to the transverse gust. Let  $\dot{s}$ ,  $\dot{h}$ , and  $\dot{\theta}_g$  be the surge rate, plunge rate, and pitch rate, respectively. The

downwash can be expressed as [41, 42]

$$W(v,t) = (\dot{s} - u_x(v,t))\sin\theta + (\dot{h} - u_z(v,t))\cos\theta + \dot{\theta}\left(\frac{c}{2}(1-\cos v) - x_C\right) + w_{\text{ind}}(v,t),$$
(3)

where the  $u_x$  and  $u_z$  terms are the external flow in the x and z directions of the inertial reference frame, respectively. The positive x direction is aligned with the direction of travel for the wing, and the positive z direction is downward according to the convention of aircraft flight dynamics. The transverse gust flow is captured by the  $u_z$  term. The induced velocity components  $u_{\text{ind}}$  and  $w_{\text{ind}}$  are contributions from previously shed LEV and TEV discrete vortices in the flow field, expressed in the body frame.

At each time step, the DVM determines the distribution of vorticity at a discrete set of points along the chord of the airfoil in order to enforce no flow across the chord line. The DVM also sheds new vortices into the flow with strengths that are calculated to satisfy the Kelvin condition, which ensures that there is no net change in circulation in the airfoil and external flow field [25, 41]. The DVM sheds vorticity at the trailing edge at each time step, and it sheds vorticity at the leading edge if the LESP value is above the critical value LESPc.

To determine the strengths of shed vortices, note that the total bound circulation can be determined by integrating  $\gamma$  along the chord to give,

$$\Gamma_B(t) = \int_0^{\pi} \gamma(\nu, t) \frac{c}{2} \sin \nu d\nu = Uc\pi \left[ A_0(t) + \frac{A_1(t)}{2} \right]. \tag{4}$$

If shedding occurs only at the trailing edge for the *j*th time step, the strength of the shed TEV can be determined from the change in bound circulation since the last time step such that

$$\Gamma_{\text{TEV}}^{j} = \Gamma_{B}^{j-1}(t) - \Gamma_{B}^{j}(t). \tag{5}$$

Note that  $\Gamma_B^j$  is also unknown and depends on  $\Gamma_{TEV}^j$ . Newton-Raphson iteration is often applied to solve for these two quantities [24, 25]. However, iteration can be avoided by noting that the TEV strength  $\Gamma_{TEV}^j$  can be linearly factored out of total bound circulation  $\Gamma_B^j$  and solved for according to [41],

$$\Gamma_{\text{TEV}}^{j} = \frac{\Gamma_{B}^{j-1} + c \int_{0}^{\pi} \mathcal{W}^{0}(1 - \cos \nu) d\nu}{1 - c \int_{0}^{\pi} \mathcal{W}'_{\text{TEV}}(1 - \cos \nu) d\nu}.$$
(6)

Equation 6 introduces two manipulated downwash terms:  $W'_{TEV}$  is the downwash induced by a unit strength vortex located at the position of the newly shedding vortex, and  $W^0$  is the downwash induced by all other vortices in the flow field, the airfoil kinematics, and external flow effects. Once the strength of the latest TEV is determined, the downwash and Fourier coefficients can be obtained.

For shedding at the leading edge, the LESP value is associated with the leading Fourier coefficient  $A_0$  [25]

$$LESP(t) = A_0(t). (7)$$

If the LESP value is greater than the critical value LESPc, vortices release from both edges of the airfoil, and the strength of LEV can be determined by forcing the current LESP value to LESPc at each time step. For simultaneous shedding, the strengths the LEV and TEV can be determined by a similar approach to the calculation used to obtain Eqn. (6). This process leads to the linear system of equations

$$[A] \begin{Bmatrix} \Gamma_{\text{TEV}}^{j} \\ \Gamma_{\text{LEV}}^{j} \end{Bmatrix} = [B], \tag{8}$$

where

$$[A] = \begin{bmatrix} 1 - c \int_0^{\pi} W'_{\text{TEV}} (1 - \cos v) dv & 1 - c \int_0^{\pi} W'_{\text{LEV}} (1 - \cos v) dv \\ \int_0^{\pi} W'_{\text{TEV}} dv & \int_0^{\pi} W'_{\text{LEV}} dv \end{bmatrix}$$
(9)

and

$$[B] = \begin{bmatrix} \Gamma_B^{j-1} + c \int_0^{\pi} W_{\text{TEV}}^0 (1 - \cos \nu) d\nu \\ -\pi U_{\text{ref}} \text{LESP}_c - \int_0^{\pi} W^0 d\nu \end{bmatrix}, \tag{10}$$

where  $W'_{LEV}$  is the downwash induced by a unit strength vortex at the shedding location for the new LEV. Once the strengths of the newly shed vortices are determined, their induced flow can be used to compute the downwash, Fourier coefficients, vortex dynamics, and forces on the airfoil.

The inertial-frame components of the induced velocity at a point (x, z) due to a de-singularized discrete vortex at  $(x_i, z_j)$  are [43]

$$u_{j} = \frac{\Gamma_{j}}{2\pi} \frac{z - z_{j}}{\sqrt{[(x - x_{j})^{2} + (z - z_{j})^{2}]^{2} + r_{c}^{4}}}$$

$$w_{j} = \frac{\Gamma_{j}}{2\pi} \frac{-(x - x_{j})}{\sqrt{[(x - x_{j})^{2} + (z - z_{j})^{2}]^{2} + r_{c}^{4}}}.$$
(11)

The strength of the  $\alpha$ th point vortex is  $\Gamma_j$ , and  $r_c$  is the radius of the vortex core. SureshBabu et al. [41] suggest setting  $r_c$  to approximately 1.3 times the average spacing between vortices. The induced velocity contribution  $w_{\text{ind}}$  in 3 results from summing the  $u_j$  and  $w_j$  contributions due to shed vortices in (11) and transforming the flow components to the body frame.

#### **B.** Force Calculation

The forces on the airfoil are calculated using a pressure-based approach. The pressure distribution along the airfoil is given by the unsteady Bernoulli equation [44]

$$\Delta p(x) = \rho \left[ (U\cos\theta + \dot{h}\sin\theta + u_{\rm ind}(x))\gamma(x) + \frac{\partial}{\partial t} \int_{x'=0}^{x} \gamma(x')dx' + \dot{\Gamma}_{\rm LEV} \right],\tag{12}$$

in which the last term accounts for loading induced by LEV shedding. The normal force per unit span in terms of the Fourier coefficients becomes [25, 44]

$$F_{N} = \rho \pi c U_{\text{ref}} \left[ (U \cos \theta + \dot{h} \sin \theta) \left( A_{0}(t) + \frac{A_{1}(t)}{2} \right) + c \left( \frac{3}{4} \dot{A}_{0}(t) + \frac{1}{4} \dot{A}_{1}(t) + \frac{1}{8} \dot{A}_{2}(t) \right) \right] + \rho \int_{0}^{c} u_{\text{ind}}(x) \gamma(x, t) dx + \rho c \dot{\Gamma}_{\text{LEV}}.$$
(13)

The suction force per unit span is [44]

$$F_S = \rho \pi c U_{\text{ref}}^2 A_0^2. \tag{14}$$

The detailed derivation of the force calculation is omitted but is available in [25, 44]. Dividing the forces by  $\rho c U_{\text{ref}}^2/2$  provides the normal and suction force coefficients  $C_N$  and  $C_S$ . Then, the lift and drag coefficients are

$$C_L = C_N \cos \theta + C_S \sin \theta$$

$$C_D = C_N \sin \theta - C_S \cos \theta.$$
(15)

This work studies only the lift coefficient  $C_L$  during a gust encounter, however other force components could potentially be targets for force regulation.

Hemati et al. [45] previously noted that DVM models tend to over-predict the lift force. Dividing Eqns. (13) and (14) by the dynamic pressure  $\rho c U_{\rm ref}^2/2$  leads to the  $2\pi$  lift-coefficient slope from classical thin-airfoil theory. In [36], the authors replaced the  $2\pi$  coefficient with the empirical coefficient obtained from the steady-lift curve measured in experiments. The same modification is made in this paper to provide realistic lift values. Note that this modification only scales the output of the DVM simulation, which is a placeholder for experimental evaluation, and it does not alter the SIMO method. In particular, the SIMO method does not require empirical values.

## C. Simulation of a Gust Encounter for a Non-maneuvering Wing

This section pairs the LDVM simulation of a wing's shed vorticity with a prescribed velocity profile of a transverse gust. The gust profile is based on time-averaged measurements of an experimental gust setup in a water towing tank at the University of Maryland, according to data from [36]. A gray line in Fig. 1 provides the gust profile, which has a trapezoidal shape and an approximate gust ratio of  $GR = V_{max}/U = 0.7$ . Within the LDVM simulation, the gust profile influences the downwash calculation in (3), which in turn, influences vortex shedding and the forces on the wing. The

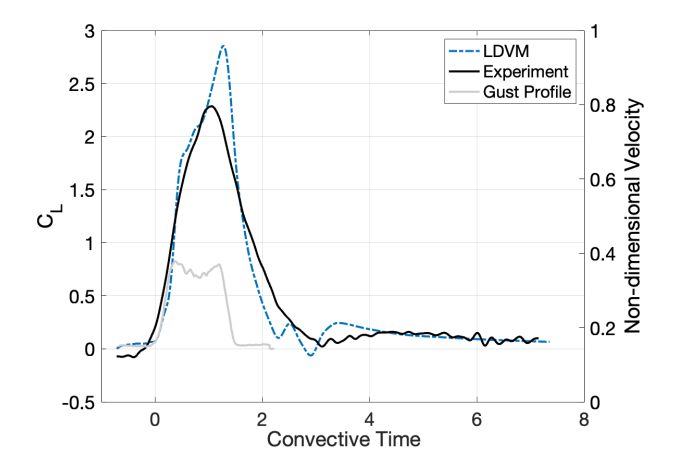


Fig. 1 Lift coefficient of a non-maneuvering wing during an encounter with a trapezoidal, transverse gust (experimental data taken from [36])

gust profile is assume to be unaffected by the wing, since Sedky et al. [26] have shown that simulated gust deformation does not significantly alter the forces when compared to an encounter with a non-deforming gust profile at a similar Reynolds number and gust ratio. Figure 1 also shows the lift coefficient during an LDVM simulation of a gust encounter for a non-maneuvering wing at zero angle of attack. The simulation extends beyond the time when the trailing edge of the wing exits the gust to ensure that the lift force returns to its steady-state value by the end of the simulation. As shown in Figure 1, the wing experiences a lift overshoot after the leading edge enters the gust, and it lasts even after the trailing edge of the wing exits the gust. The lift coefficient then gradually returns to zero. Prior to one convective time, the lift values predicted by the LDVM (blue dashed line) show good agreement with experimental measurements (black line) taken in [36]. The experiments occurred with a NACA0012 wing of chord c = 0.102m and an effective aspect ratio of 5. The towing speed was 0.115m/s, and the Reynolds number was Re= 12,000. The LDVM over-predicts the peak value, but the remainder of the curve is generally close to the experimental data. For this paper, the LDVM serves as the test model in place of higher-fidelity simulations or experiments. Numerical experiments using the LDVM for maneuver optimization appear in Sec. VI.

# IV. Iterative Maneuver Optimization

The Iterative Maneuver Optimization (IMO) developed in [36] addresses the issue that optimal control profiles derived using a surrogate model of a wing-gust encounter fail to achieve their expected performance in experiments or higher-fidelity simulations due to the presence of unmodeled effects. The IMO method uses deviations of experimental measurements from the predicted aerodynamic forces to update the control signal. Through iterated applicable of this process, the control performance improves. This section briefly reviews the IMO method.

Let u(t) with  $t \in [t_0, t_f]$  be a scalar control signal between start time  $t_0$  and end time  $t_f$  that actuates the wing, and let  $y_{\text{model}}$  represent a scalar force component of interest, such as lift. This paper investigates pitch and plunge accelerations individually as control inputs in Sec. VI. The IMO method requires a model for the dynamics of the system's state vector x in the form,

$$\dot{\mathbf{x}} = f\left(\mathbf{x}, u, t; \boldsymbol{\mu}\right) \tag{16a}$$

$$y_{\text{model}} = h\left(\mathbf{x}, u, t; \boldsymbol{\mu}\right),\tag{16b}$$

where f and h may be nonlinear functions, and  $\mu$  is a vector containing any empirical terms needed by the model. Equation (16) represents a surrogate model of the true dynamics of the fluid-wing interaction. The functions f and h are assumed to be differentiable with respect to x and u for optimal control calculations that are part of the IMO method. In prior work [36], an mGK model served as the surrogate model, and it contained numerous empirical terms that needed to be fit to the wing prior to use.

The IMO method performs an optimal control calculation to find a control signal u that minimizes the performance

index

$$J(u) = \frac{1}{2} \int_{t_0}^{t_f} \left( y_{\text{model}}^{(i)}(\mathbf{x}, u, t) - y_{\text{ref}}^{(i)} \right)^2 dt, \tag{17}$$

subject to the dynamics of the surrogate model (16). The superscript (i) denotes that a signal comes from the ith iteration of the IMO method. On the first step of IMO, minimizing (17) regulates the model output  $y_{\text{model}}^{(1)}$  to the constant value  $y_{\text{ref}}^{(1)}$ . On subsequent iterations,  $y_{\text{ref}}^{(i)}$  becomes a non-constant signal that surrogate system should track. A candidate optimal control can be obtained by solving the first-order optimality conditions [42]

$$\dot{\mathbf{x}} = \left(\frac{\partial H}{\partial \lambda}\right) \quad \text{with} \quad \mathbf{x}(t_0) = \mathbf{x}_0$$
 (18a)

$$\dot{\mathbf{x}} = \left(\frac{\partial H}{\partial \lambda}\right) \qquad \text{with} \quad \mathbf{x} (t_0) = \mathbf{x}_0$$

$$\dot{\lambda} = -\left(\frac{\partial H}{\partial \mathbf{x}}\right)^T \quad \text{with} \quad \lambda (t_f) = \mathbf{0}$$
(18a)

$$0 = \frac{\partial H}{\partial u}. ag{18c}$$

Standard algorithms from optimal control theory (e.g., see [46]) solve the first-order optimality conditions (18). The authors' prior work [42] modifies these conditions to include terminal state constraints, which are useful if the wing is required to be in a particular configuration (i.e., position and orientation) at the end of the maneuver.

A control u obtained by optimizing (17) over the surrogate model is tested in an experiment or high-fidelity simulation to produce the output signal  $y_{\text{test}}^{(i)}(t)$  with  $t \in [t_0, t_f]$ . Although the model output  $y_{\text{model}}^{(i)}$  is close to the reference value  $y_{\text{ref}}^{(i)}$  as a result of the optimal control calculation, the output  $y_{\text{test}}^{(i)}$  deviates from  $y_{\text{ref}}^{(i)}$  due to unmodeled effects. The difference between the test (i.e., measured) output and the model output in the ith iteration is

$$\Delta y^{(i)} = y_{\text{test}}^{(i)} - y_{\text{model}}^{(i)}.$$
 (19)

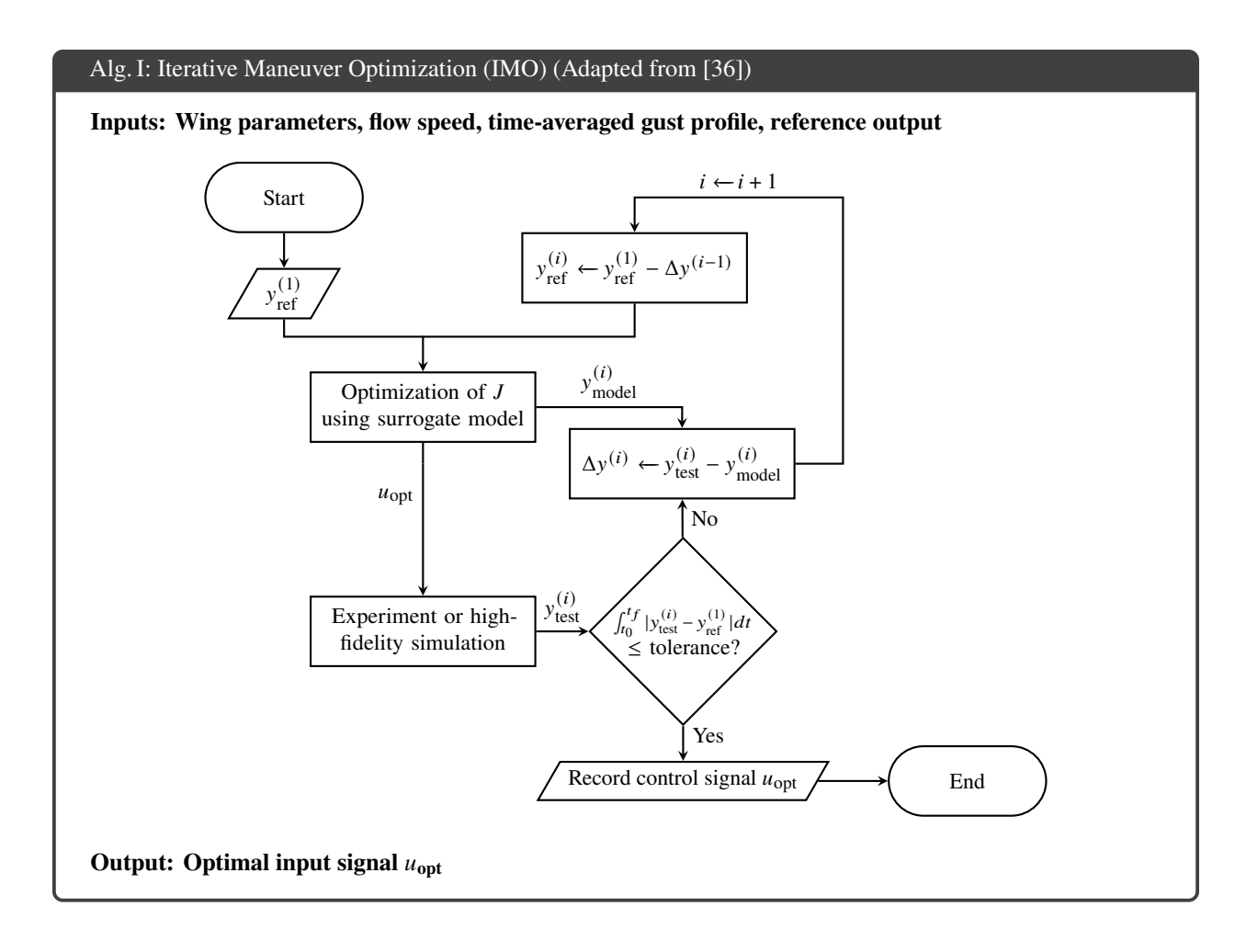
After completion of both surrogate optimization and testing of the control signal, if the absolute difference between the test signal and the reference  $y_{ref}^{(1)}$  integrated over the time period is less a desired tolerance, then acceptable regulation has been achieved. Otherwise, the iteration counter is incremented such that i = i + 1 and the IMO process can continue.

The output error (19) can be used to find a new control signal in the next iteration by updating the reference signal for the optimal-control calculation to be

$$y_{\text{ref}}^{(i)} = y_{\text{ref}}^{(1)} - \Delta y^{(i-1)}.$$
 (20)

IMO minimizes performance index (17) to track the new reference signal (20). Then, the updated optimal control profile can again be tested in experiment or high-fidelity simulation. To examine Eqns. (19) and (20) further, consider a force measurement  $y_{\text{test}}^{(i)}$  at a given time that is less than the value predicted by the model  $y_{\text{model}}^{(i)}$  due to unmodeled effects. Eqns. (19) and (20) would increase  $y_{\text{ref}}$  for the next iteration, and the subsequent optimal-control calculation would seek a control that produces a larger model output  $y_{\text{model}}$  at that time. If the surrogate model generally agrees with the true fluid dynamics, the subsequent test value  $y_{\text{test}}$  should increase as well under the same control input, thereby bringing it closer to the initial reference value  $y_{\text{ref}}^{(1)}$ . This process repeats until the measured output signal  $y_{\text{test}}$  approaches the constant, initial reference value  $y_{\text{ref}}^{(1)}$ . Algorithm V illustrates the IMO procedure.

The inputs to the algorithm are a time-averaged profile of the transverse gust, a surrogate model of the wing-gust interaction, and the reference output value for force regulation. The output of the algorithm is the optimal control input signal that achieves lift regulation. In prior work [36], the authors created a surrogate model by modifying a Goman-Khrabrov model to include effective angle of attack. Effective angle of attack allows for incorporation of a prescribed velocity field representing the gust. The output of the mGK model is the lift coefficient  $C_L$ , and the control input is pitch acceleration  $\ddot{\theta}$ . Using a DVM, the authors showed that the IMO method converges to produce an optimal, lift-regulating maneuver. Together with collaborators, the authors also experimentally tested the result in a water towing tank with a gust generator and showed that the IMO method approximately regulates lift in only a few iterations, similar to the numerical simulations. However, the final experimental iterations contained deviations from the reference lift that oscillated for further iterations. The authors showed that the same effect could be replicated in DVM by lowering the critical value of the leading edge suction parameter (i.e., the threshold for shedding at the leading edge) to make the leading edge more sensitive to shedding. Despite these small oscillations, experiments validated that the IMO method produces a lift-regulating pitch maneuver.



# V. Simplified Iterative Maneuver Optimization

This section introduces the Simplified Iterative Maneuver Optimization (SIMO) method. SIMO uses Theodorsen's lift model to eliminate the empirical terms in the mGK surrogate model and remove the requirement for a time-average profile of the gust. This change greatly reduces the experimental effort necessary before implementing the method. SIMO also replaces the costly optimization step in IMO with a more efficient simulation based on closed-loop tracking control of Theodorsen's lift model.

In [36], the IMO method uses a nonlinear mGK model that compares well to experimental lift measurements in the amplitude and duration of the the lift overshoot for a non-maneuvering wing. However, the authors note that the mGK model also has a noticeable delay in the lift response when compared to experimental data. Despite this delay, IMO method is able to achieve accurate lift regulation. This observation suggests that the surrogate model does not need to be highly accurate, but simply adequate at capturing general trends of the system's response. A linear dynamic model may be sufficient when applied within the IMO framework.

One such linear dynamic model of lift is Theodorsen's unsteady lift model. Theodorsen's model predicts the lift coefficient of a wing undergoing pitching and plunging maneuvers based expressions for added-mass and circulatory effects derived using potential-flow theory. Theodorsen's lift model is [47]

$$C_L = \pi b \left( \frac{\dot{\alpha}}{U} + \frac{\ddot{h}}{U^2} - \frac{ba\ddot{\alpha}}{U^2} \right) + 2\pi C(s) \left[ \frac{\dot{h}}{U} + \alpha + b \left( \frac{1}{2} - a \right) \frac{\dot{\alpha}}{U} \right], \tag{21}$$

where b is the half-chord length, U is the steady, free-stream velocity,  $\alpha$  is the geometric angle of attack,  $\dot{h}$  is the plunge rate, and a is the location of the pitch axis in semi-chords (e.g., a=-1 indicates pitching about the leading edge and a=1 is pitching about the trailing edge). C(s) is a generalized version of *Theodorsen's function*, which is a complex-valued function that determines the effect of the trailing-edge wake on the circulatory contribution to the unsteady airloads [47]. This version of Theodorsen's function is generalized because it allows for arbitrary airfoil

motions in addition to the sinusoidal motions originally considered by Theodorsen. There are several approximations to C(s), and this paper uses R.T. Jones's approximation [17, 37, 48]

$$C(s) = \frac{0.5s^2 + 0.2808s + 0.01365}{s^2 + 0.3455s + 0.01365},$$
(22)

where s is the Laplace variable. Using Theodorsen's model, Brunton and Rowley [37] calculate transfer functions from the pitch and plunge inputs to the lift coefficient output. Taking the Laplace transform  $\mathcal{L}\{\cdot\}$  of Eqn. (21) and separating the pitch and plunge acceleration inputs yields

$$\mathscr{L}\{C_L\} = \underbrace{\left(\frac{\pi b}{U}\left(\frac{1}{s} - ba\right) + 2\pi C(s)\left[\frac{1}{s^2} + \frac{b}{Us}\left(\frac{1}{2} - a\right)\right]\right)}_{G_{\alpha}(s)} \mathscr{L}\{\ddot{a}\} + \underbrace{\left(\frac{\pi b}{U^2} + C(s)\frac{2\pi}{Us}\right)}_{G_{h}(s)} \mathscr{L}\{\ddot{h}\},\tag{23}$$

where the transfer function  $G_{\alpha}(s)$  predicts the lift coefficient due to the pitch input, and  $G_h(s)$  predicts the lift coefficient due to the plunge input. These transfer functions can serve as surrogate models for the wing.

The IMO method uses the surrogate model to generate an optimal input profile. For a constant lift coefficient reference input, the optimal control problem is a regulation problem. In subsequent iterations of IMO, the optimal control problem becomes a tracking problem because the surrogate model is required to track a reference lift signal that changes in time since it has been altered by the previous IMO iteration. The optimal control formalism and a gradient solution algorithm are necessary in IMO because the regulation and tracking problems use an mGK model, which is a nonlinear surrogate model. Since the optimization calculations are time-consuming, in the previous work [36], the authors noted that high-gain proportional feedback was capable of producing the optimal solution with less computation time. This observation suggests that a feedback control strategy may be able to provide the necessary tracking of the reference lift signal without the need for optimization. Instead, a controller that can adequately track the reference lift coefficient signal is all that is needed.

There are many approaches to design a tracking controller that can minimize deviations between  $C_{L,\text{model}}$  and  $C_{L,\text{ref}}$ . One of the most common approaches is to use Proportional-Integral-Derivative (PID) control to compensate for the errors between the model output and the reference output. The control law can be expressed as

$$u(t) = K_p \epsilon(t) + K_i \int_0^t \epsilon(\tau) d\tau + K_d \frac{d\epsilon(t)}{dt}, \tag{24}$$

where  $K_p$ ,  $K_i$ ,  $K_d$  are non-negative, constant gains corresponding to the proportional, integral, and derivative terms, respectively, and  $\epsilon = C_{L,\text{ref}}^{(i)} - C_{L,\text{model}}^{(i)}$  is the tracking error. The control gains can be tuned in the closed-loop plant to make the model output closely match the reference signal. Note that it is not necessary to have all three terms in the PID controller. Only the proportional and integral terms are needed for good tracking of the Theodorsen lift model.

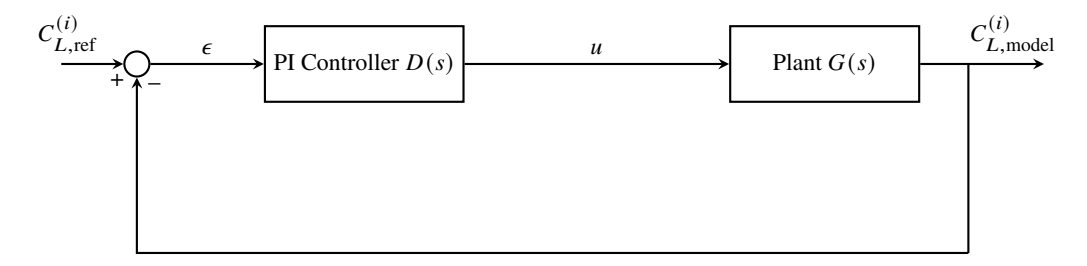


Fig. 2 Closed-loop block diagram of the surrogate model

Figure 2 shows the block diagram for closed-loop tracking control of Theodorsen's model with unity feedback. The Plant G(s) represents Theodorsen's lift model, and the controller is a Proportional-Integral (PI) controller shown as D(s), which is the Laplace transform of Eqn. (24) with  $K_d = 0$ . Since this paper considers pitch and plunge acceleration inputs individually, the plant G(s) represents either the  $G_{\alpha}(s)$  or  $G_h(s)$  transfer function, depending on the chosen input.

The transfer function from the reference  $C_{L,ref}$  to the optimal maneuver u can be computed based on the closed-loop system in Figure 2 to be

$$P(s) = \frac{\mathcal{L}\{u(t)\}}{\mathcal{L}\{C_{L,\text{ref}}(t)\}} = \frac{D(s)}{1 + G(s)D(s)}.$$
 (25)

Transfer function (25) can be used to find a control input u(t) that causes the Theodorsen model to track the reference signal  $C_{L,ref}(t)$ . The MATLAB command 1sim readily implements this calculation to find u(t), given  $C_{L,ref}(t)$ .

The controller D(s) should be tuned such that the closed-loop system P(s) provides adequate tracking. If the output of the surrogate model  $C_{L,\text{model}}^{(i)}(t)$  identically tracks  $C_{L,\text{ref}}^{(i)}(t)$ , then an additional simplification to the IMO method is possible. Substituting Eqn. (19) into Eqn. (20) and replacing  $C_{L,\text{model}}^{(i-1)}$  with  $C_{L,\text{ref}}^{(i-1)}$  yields the reference signal update

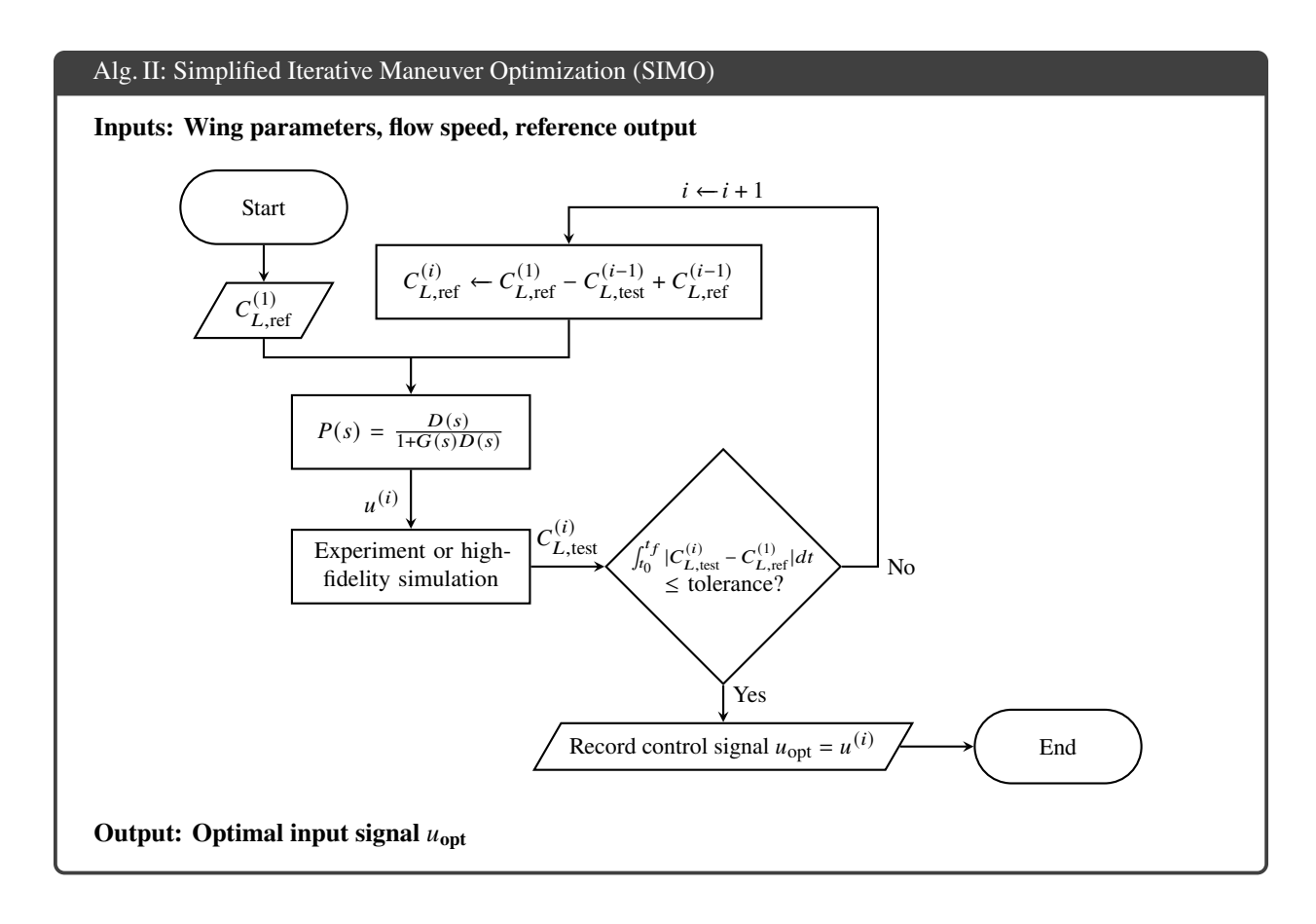
$$C_{L,\text{ref}}^{(i)} = C_{L,\text{ref}}^{(1)} - C_{L,\text{test}}^{(i-1)} + C_{L,\text{ref}}^{(i-1)}.$$
(26)

Combining these simplifications results in the Simplified IMO (SIMO) algorithm, which appears in Alg. II.

The surrogate model in SIMO is the Theodorsen's unsteady lift model with a PI controller that tracks the reference lift signal  $C_{L,\text{ref}}^{(i)}$ . Although versions of Theodorsen's model with empirical factors exist (e.g., see [37]), the original model is derived from potential flow theory and does not contain empirical factors. Since the iterative process of updating the reference signal can compensate for some model inaccuracies, this paper uses the original form of Theodorsen's lift model to avoid empirical terms in the surrogate model. Treatment of the gust as a disturbance further reduces empirical fitting, because it eliminates the need for prior knowledge of the gust profile in the surrogate model.

In the SIMO method, the wing discovers the gust on the first iteration during collection of  $C_{L,\mathrm{test}}^{(1)}$ . Unlike the IMO method, for which the initial maneuver is based on optimal regulation of the surrogate mGK model, SIMO does not maneuver the wing on the first iteration. This paper assumes that the wing operates at the reference lift value  $C_{L,\mathrm{ref}}^{(1)}$  prior to the gust encounter. Since the surrogate model does not contain gust effects, the PI controller continues to hold the wing's initial configuration for the duration of iteration 1. The gust acts as an additive output disturbance that occurs in the experiment or high-fidelity simulation and causes the lift to differ from the expected response. After the reference lift signal is disturbed by the first test run, the PI controller acts to track an updated reference lift signal that encodes disturbance information on the next iteration. The SIMO method proceeds with additional iterations until  $C_{L,\mathrm{test}}^{(i)}$  matches  $C_{L,\mathrm{ref}}^{(1)}$  within an acceptable tolerance. The relative change in the output between  $C_{L,\mathrm{test}}^{(i)}$  and  $C_{L,\mathrm{test}}^{(i-1)}$  should also be monitored to identify occurrences of oscillations that prevent further decrease in the error.

This paper applies the SIMO method to the problem of a wing encountering a transverse gust. However, SIMO may also be applicable to other problems in fluid dynamics that focus on lift regulation via wing maneuvering, provided that the external flow field can be reliably replicated in each iteration of the experiments.



# **VI. Numerical Experiments**

This section numerically implements the SIMO method from Sect. V in LDVM simulations of transverse gust encounters to produce optimized maneuvers for pitch or plunge acceleration inputs.

## A. Pitch Maneuver Optimization

In the authors' prior work on the IMO method [36], the wing generally performed a pitch-down then pitch-up maneuver to mitigate the lift overshoot during a transverse gust encounter. The authors found that for an LESPc value of 0.18, the IMO method converges in simulation to nearly perfect regulation of  $C_L$  to zero within seven iterations. For an LESPc value of 0.12, LEVs more readily shed at the leading edge. In particular, this LESPc value produces more leading-edge shedding on the high-pressure side of the wing while the wing pitches down to its furthest extent. The additional LEV shedding is associated with small spikes in the lift response and oscillation in maneuver updates, preventing further convergence of the solution after several iterations. Therefore, the present paper focuses on the more challenging case of LESPc= 0.12 for investigation of the SIMO method and comparison to the IMO method.

To numerically implement SIMO for a pitch acceleration input, the simulation parameters are set to match experimental values in the previous work [36]. The freestream flow speed, which is based on the towing speed of the wing, is 0.115m/s, and the gust ratio is approximately GR= 0.7. The chord length of the wing is c = 0.102m. The pitch axis location is on the chord line at a = -0.17. The control input is pitch acceleration  $\theta$ , and the output is lift coefficient  $C_L$ . To generate control signals based on tracking control of the surrogate model, the proportional and integral control gains in (24) were selected to be  $K_p = 1.4$  and  $K_i = 435.24$ , respectively, for all iterations. These values were selected using the pidtune command in MATLAB with a 0dB open-loop crossover frequency of 50Hz.

Figure 3 presents pitch maneuver optimization using the SIMO method. No maneuvering occurred on the first iteration, producing a lift-overshoot profile as shown in Fig. 3(a). The second iteration directly applied a strong pitch-down maneuver to counteract the lift overshoot. However, this maneuver was too strong and produced a large lift undershoot instead. In iteration 3, the wing reduced the maneuvering amplitude, eliminating the lift undershoot and producing less lift overshoot than the non-maneuvering case. Iterations 3 through 7 continued to reduce deviations from

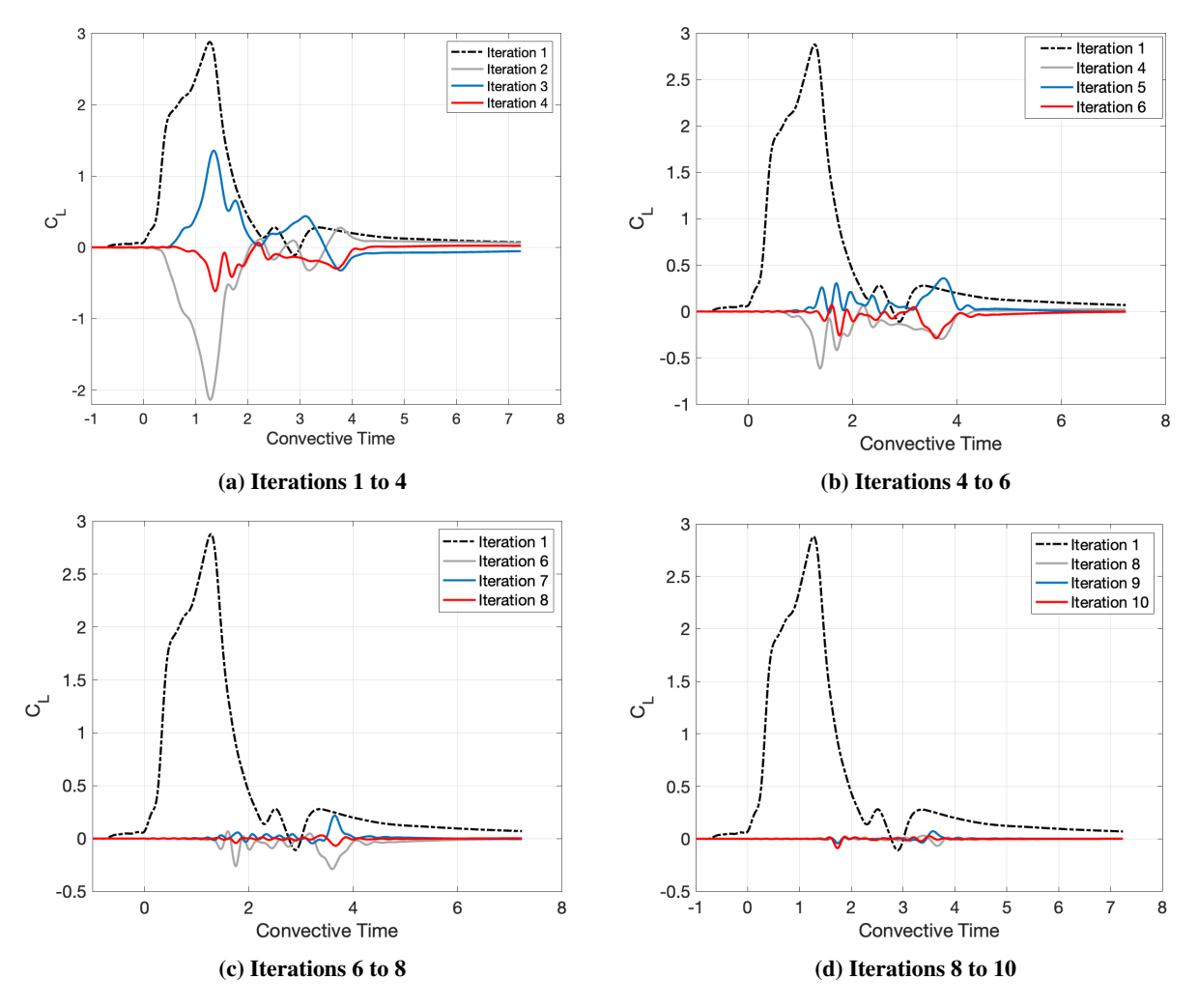


Fig. 3 LDVM simulation results of the SIMO method for a pitch acceleration input

the desired value of  $C_L = 0$ . Iteration 8 reached a nearly optimal result. Iterations 9 and 10 made slight enhancements along the output lift curve, however, small oscillations in the solution at  $t^* = 1.8$  were noticed and the simulation was terminated due to a lack of improvement beyond iteration 10. The largest absolute deviation in lift coefficient for iteration 10 was 0.08, which represents a 97% reduction in maximum lift deviation compared to iteration 1.

Figure 4 shows the angle of attack maneuver for each iteration, as well as the pitch acceleration input that generates the maneuver. The optimized maneuver on iteration 10 is a pitch-down, then pitch-up maneuver as shown in Fig. 4(a). Figure 5 compares the optimized lift responses of the IMO method (blue line) and the SIMO method (red line). These lines are taken from iteration 10 for each method, and it is clear that SIMO method performed better than the IMO method at generating a lift-regulating maneuver. The simpler Theodorsen model may be better suited than the mGK model to serve as a surrogate in iterative maneuver optimization.

These simulation results show that the SIMO method is capable of optimizing the maneuver of a pitching wing in a transverse gust for lift regulation. Similar to IMO, SIMO also exhibits oscillation in the optimized maneuver after several iterations. Oscillation of the maneuver is the subject of ongoing work for improvement of the method. Nevertheless, the SIMO method rapidly generates an optimized maneuver in only a few iterations of maneuvering in the LDVM simulation. Further, SIMO outperforms the IMO method for this simulation and does so without prior knowledge of the gust profile.

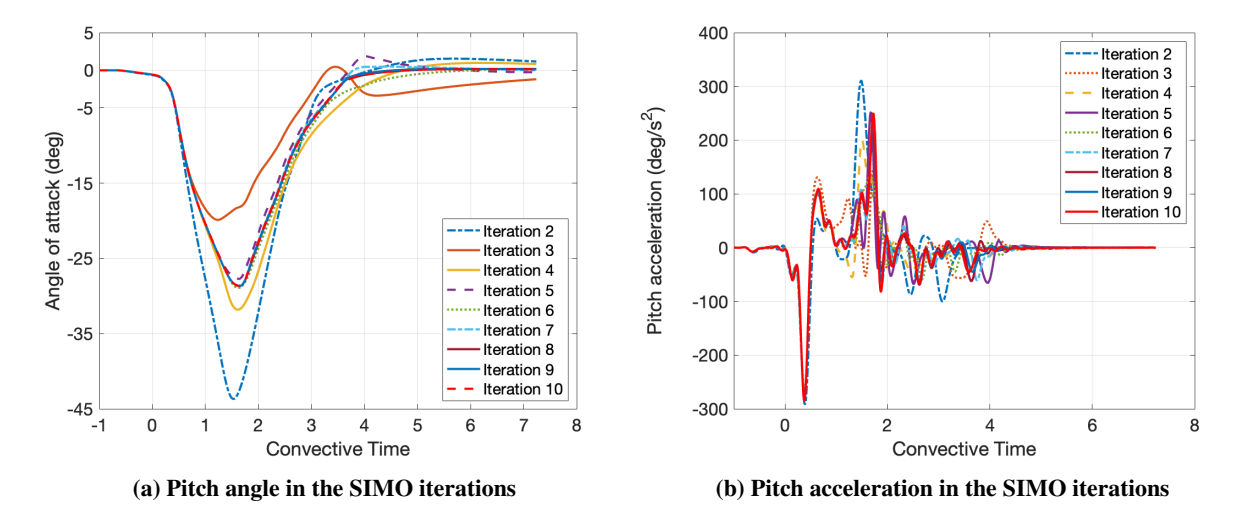


Fig. 4 Results of the SIMO method for a pitch acceleration input

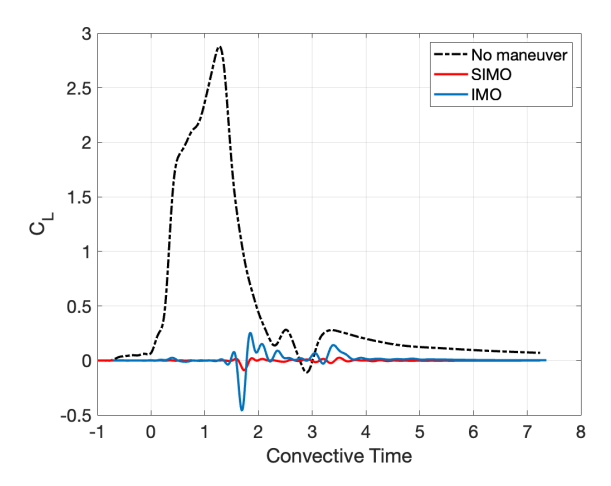


Fig. 5 Comparison of lift regulation for maneuvers generated using the IMO and SIMO methods

# **B. Plunge Maneuver Optimization**

This numerical experiment investigates lift regulation using a plunge acceleration input to derive a plunge maneuver. Theodorsen's lift model decomposes into the transfer functions from pitch and plunge inputs to the lift output in Eqn. (23). To examine plunge individually, the pitch input was set to zero. The simulation parameters for wing geometry and flow conditions, including the LESPc value, matched those from the numerical experiment in Sec. VI.A for pitch maneuvering. The PI controller in the surrogate tracking model was tuned to control gains of  $K_p = 0$  and  $K_i = 4.13$  for all iterations, which shows that only integral control was active.

Figure 6 presents the lift response results for plunge maneuver optimization using the SIMO method. For iteration 1 in Fig. 6(a), the wing did not maneuver, which provided the same open-loop gust response seen in the previous numerical experiment. For iteration 2, the plunge motion derived by SIMO significantly reduced the largest absolute deviation in lift coefficient to 0.4, which is an 86% reduction from the non-maneuvering wing's lift overshoot. Notably, the plunge maneuver from iteration 2 mitigated the disturbance better than the pitching maneuver from iteration 2 in Fig. 3(a). The remaining iterations in Figs. 6(b) and 6(c) continued to refine the performance of the plunge maneuver in small increments. By iteration 8, the largest absolute deviation of the lift coefficient was 0.02, which is a reduction of 99% from the open-loop lift overshoot. Within an acceptable tolerance, iteration 8 optimally regulated the lift coefficient to zero during the gust encounter through the use of a plunge maneuver. Note that the plunge maneuver required fewer iterations than the pitch maneuver to optimize, and it did not experience significant oscillation of lift spikes with continued iteration.

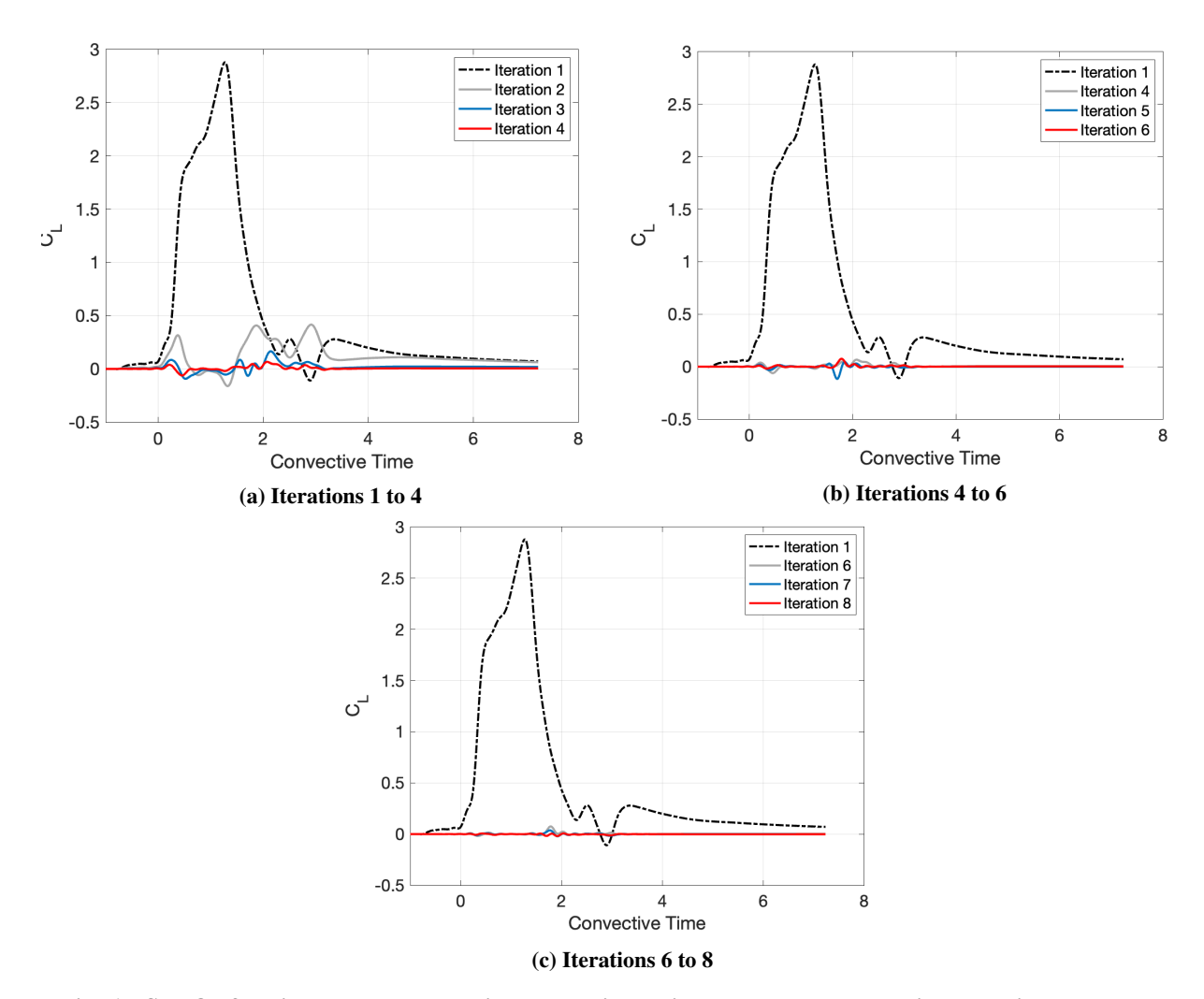


Fig. 6 SIMO of a wing-gust encounter in LDVM simulation and the corresponding plunging maneuvers.

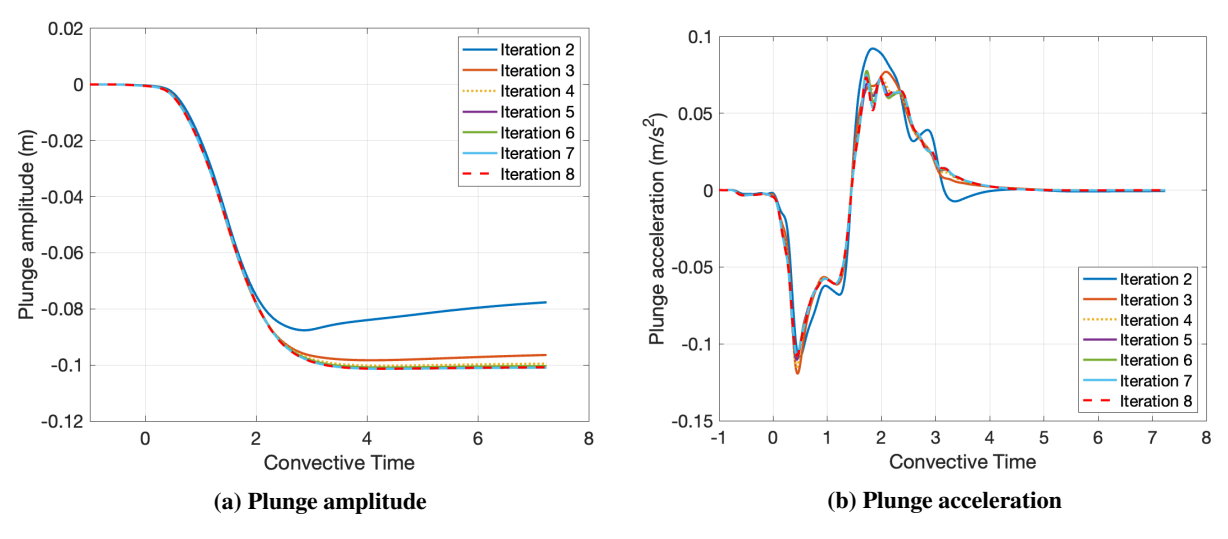


Fig. 7 SIMO of a wing-gust encounter in LDVM simulation and the corresponding plunging maneuvers

Figures 7(a) and 7(b) record the plunge amplitudes and accelerations, respectively. The plots show rapid convergence of the plunge maneuver after iteration 2. The optimal plunge maneuver can generally be described as negatively plunging (i.e., ascending) to a higher altitude and holding the new position. The wing ascended to approximately -0.1m and held that amplitude after  $t^* = 3$ . The optimal plunge input in Fig. 7(b) is negative for downward acceleration during entry into the gust and positive after exiting the gust to bring the plunge rate back to zero. In contrast to the optimized pitch maneuver, which returned the wing to its original orientation after the gust encounter, the optimal plunge maneuver held an offset altitude after the encounter. Since the angle of attack is explicitly in Theodorsen's lift model in Eqn. 21, the wing naturally returns to its initial orientation at the end of the pitch maneuver for lift regulation. That is, when all rate-of-change terms in Eqn. 21 go to zero, the angle of attack must match the initial angle of attack for the lift value to be the same. Note that the plunge rate and plunge acceleration appear in Eqn. 21, but the plunge amplitude does not. This observation reveals a benefit of the IMO framework over the SIMO method, because IMO incorporates terminal constraints on the final configuration of the wing in the optimization portion of the mGK surrogate model.

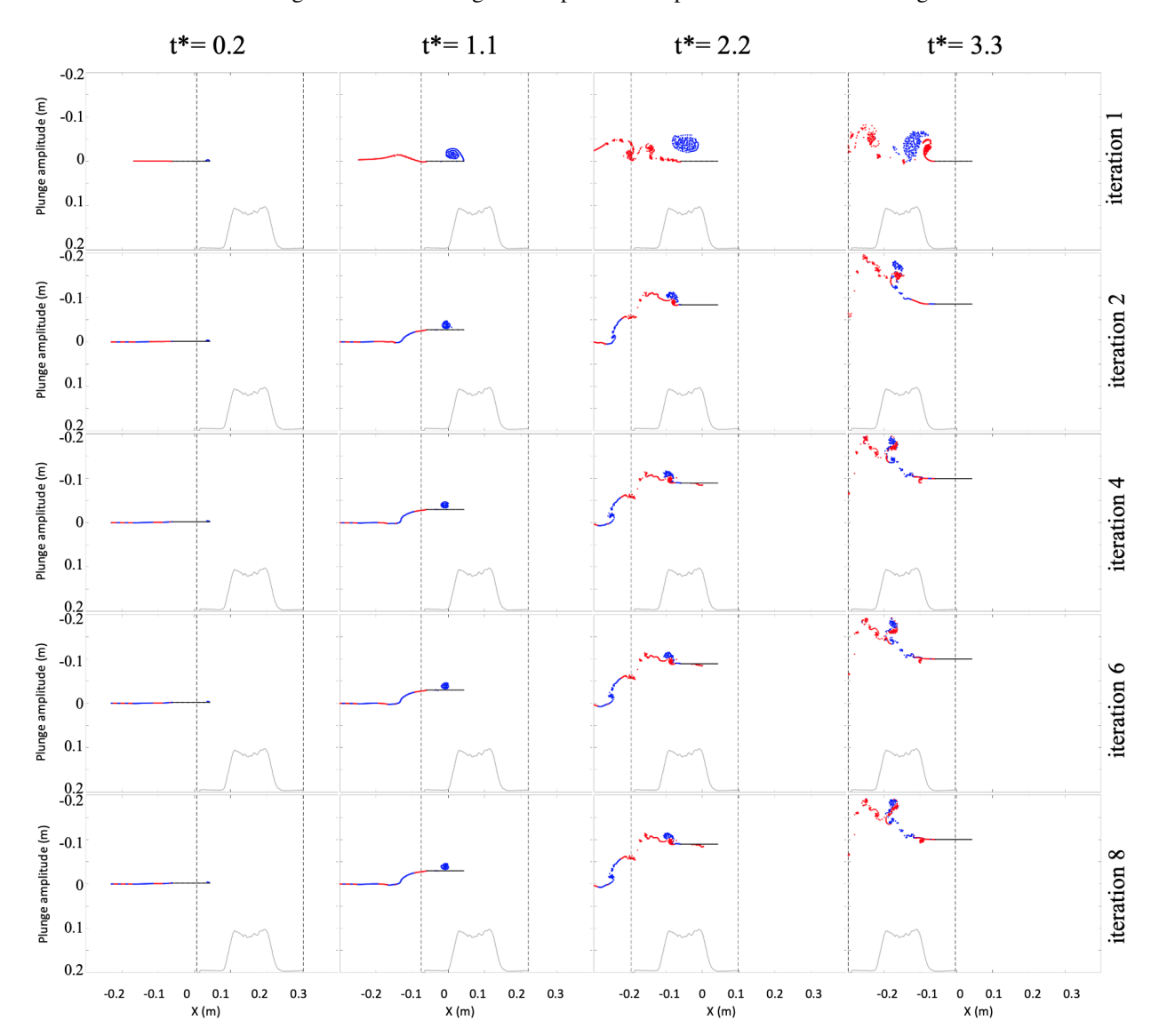


Fig. 8 Free vortices in the flow field for SIMO iterations with a plunge acceleration input

Figure 8 depicts the free vortices in the flow field for four time instants during the LDVM simulations in a reference frame that translates horizontally with the wing. Each row shows the plunge maneuver for an iteration of the SIMO method. Iteration 1 shows the non-maneuvering gust encounter. A large LEV rolls up during entry into the gust and sheds shortly after  $t^* = 1.1$ . The negative plunging or ascending motion in the SIMO iterations reduces the size of the

LEV and causes shedding of the LEV before  $t^* = 1.1$ . Also, note that at time instant  $t^* = 2.2$ , the wake from vortex shedding at the trailing edge is reduced in iteration 8 as compared to iteration 1.

After iteration 2, a small LEV advects under the high-pressure side of the wing and can be seen at  $t^* = 2.2$ . The high-pressure side LEV is often present for pitch maneuvers. Figure 9 compares the optimized pitch and plunge maneuvers at  $t^* = 2.2$ , and it shows a smaller high-pressure-side LEV appears for the plunge maneuver than the pitch maneuver. The less prominent high-pressure-side LEV may be account for the improved lift regulation of the plunge maneuver and the reduced oscillation effect near the optimal maneuver.

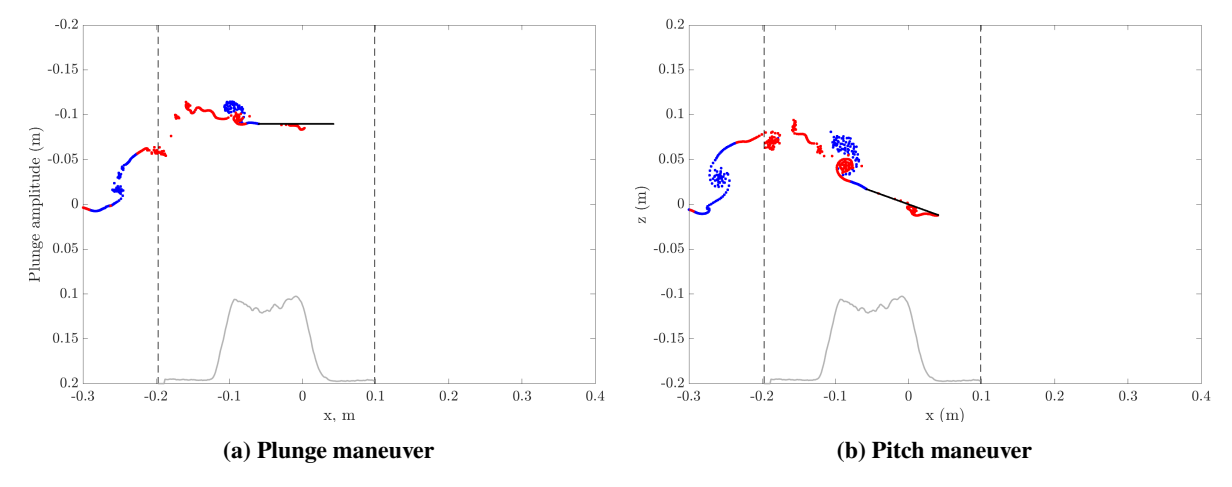


Fig. 9 Comparison of free vortices in the flow field of the LDVM simulation at  $t^* = 2.2$ 

### VII. Conclusion

This work revises and simplifies the Iterative Maneuvering Optimization (IMO) framework developed in the authors' previous work in [36]. IMO is a tool to create lift-regulating maneuvers by conducting several successive experiments or numerical simulations. A Simplified Iterative Maneuvering Optimization (SIMO) method is introduced and tested in this paper with numerical simulations using a discrete vortex model. The SIMO method replaces optimization over a surrogate model in the IMO method with Theodorsen's unsteady lift model combined with a PI controller to track a reference lift signal. Additionally, the new SIMO approach does not require any preliminary experimental effort to obtain empirical parameters for a surrogate model or the time-averaged profile of the external flow field, which is required by IMO. These changes significantly simplify the IMO framework. However, the SIMO framework currently lacks the ability to constrain the wing's position and orientation at the final time, which is possible using IMO.

The SIMO method can be used for pitching or plunging maneuvers, and numerical experiments successfully generate the optimal inputs for lift regulation during a transverse gust encounter for a trapezoidal gust profile. The wing applies a pitch-down, then pitch-up maneuver for pitch actuation and a negative plunge (i.e. ascent) motion for plunge actuation. The resulting pitch maneuver provides a 97% reduction of the maximum absolute lift response, and the plunge maneuver provides 99% reduction. Snapshots of the vorticity field of the plunge case indicate that the optimal maneuver reduces shedding of vorticity at the leading edge during the encounter. Future work will focus on experimental validation of the proposed SIMO method and examine stability analysis of the SIMO method.

# **Acknowledgments**

This work was supported by the National Science Foundation under grant CBET-2003999, monitored by program officer R. Joslin. The authors gratefully acknowledge valuable discussions and communication with Z. Chen, A. SureshBabu, A. Gopalarathnam, G. Sedky, A. Gementzopoulos, and A. R. Jones.

# References

[1] Zarovy, S., Costello, M., Mehta, A., Gremillion, G., Miller, D., Ranganathan, B., Humbert, J. S., and Samuel, P., "Experimental study of gust effects on micro air vehicles," *AIAA Atmospheric Flight Mechanics Conference*, 2010, p. 7818.

- [2] Moulin, B., and Karpel, M., "Gust loads alleviation using special control surfaces," *Journal of Aircraft*, Vol. 44, No. 1, 2007, pp. 17–25.
- [3] Moriche, M., Flores, O., and Garciá-Villalba, M., "On the aerodynamic forces on heaving and pitching airfoils at low Reynolds number," *Journal of Fluid Mechanics*, Vol. 828, 2017, pp. 395–423. https://doi.org/10.1017/jfm.2017.508.
- [4] Sedky, G., Gementzopoulos, A., Andreu-Angulo, I., Lagor, F. D., and Jones, A. R., "Physics of gust response mitigation in open-loop pitching manoeuvres," *Journal of Fluid Mechanics*, Vol. 944, 2022, p. A38. https://doi.org/10.1017/jfm.2022.509, URL https://www.cambridge.org/core/product/identifier/S0022112022005092/type/journal\_article.
- [5] Jones, A. R., Cetiner, O., and Smith, M. J., "Physics and Modeling of Large Flow Disturbances: Discrete Gust Encounters for Modern Air Vehicles," *Annual Review of Fluid Mechanics*, Vol. 54, 2021, pp. 469–493. https://doi.org/10.1146/annurev-fluid-031621-085520.
- [6] Bhatia, M., Patil, M., Woolsey, C., Stanford, B., and Beran, P., "Stabilization of Flapping-Wing Micro-Air Vehicles in Gust Environments," *Journal of Guidance, Control, and Dynamics*, Vol. 37, No. 2, 2014, pp. 592–607. https://doi.org/10.2514/1.59875, URL https://doi.org/10.2514/1.59875.
- [7] Cook, R. G., Palacios, R., and Goulart, P., "Robust gust alleviation and stabilization of very flexible aircraft," *AIAA journal*, Vol. 51, No. 2, 2013, pp. 330–340.
- [8] Oduyela, A., and Slegers, N., "Gust mitigation of micro air vehicles using passive articulated wings," *The Scientific World Journal*, Vol. 2014, 2014.
- [9] Jones, A. R., "Gust encounters of rigid wings: Taming the parameter space," *Physical Review Fluids*, Vol. 5, No. 11, 2020, p. 110513.
- [10] Ellington, C. P., den Berg, C. V., and Willmott, A. P., "Leading-edge vortices in insect flight," *Nature*, Vol. 384, No. December, 1990, pp. 626–630.
- [11] Biler, H., Badrya, C., and Jones, A. R., "Experimental and Computational Investigation of Transverse Gust Encounters," *AIAA Journal*, Vol. 57, No. 11, 2019, pp. 1–15. https://doi.org/10.2514/1.j057646.
- [12] Grubb, A. L., Moushegian, A., Heathcote, D. J., and Smith, M. J., "Physics and Computational Modeling of Nonlinear Transverse Gust Encounters," AIAA SciTech 2020 Forum, 2020. https://doi.org/10.2514/6.2020-0080, URL https://arc.aiaa.org/doi/abs/10.2514/6.2020-0080.
- [13] Andreu-Angulo, I., Babinsky, H., Biler, H., Sedky, G., and Jones, A. R., "Effect of Transverse Gust Velocity Profiles," AIAA Journal, Vol. 58, No. 12, 2020, pp. 5123–5133.
- [14] Angulo, I. A., and Babinsky, H., Unsteady Modelling of Pitching Wings for Gust Mitigation, AIAA Scitech 2021 Forum. https://doi.org/10.2514/6.2021-1999, URL https://arc.aiaa.org/doi/abs/10.2514/6.2021-1999.
- [15] Sedky, G., Jones, A. R., and Lagor, F. D., "Lift Regulation During Transverse Gust Encounters Using a Modified Goman–Khrabrov Model," AIAA Journal, Vol. 0, No. 0, 2020, pp. 1–11. https://doi.org/10.2514/1.J059127, URL https://doi.org/10.2514/1.J059127.
- [16] Xu, X., and Lagor, F. D., "Optimal Pitching in a Transverse Gust Encounter Using a Modified Goman-Khrabrov Model," AIAA AVIATION 2021 FORUM, 2021, p. 2937.
- [17] Sedky, G., "Mitigation of transverse gusts via open- and closed-loop pitching maneuvers," Ph.d. dissertation, University of Maryland, 2022.
- [18] Andreu Angulo, I., and Babinsky, H., "Negating gust effects by actively pitching a wing," AIAA Scitech 2020 Forum, 2020, p. 1057.
- [19] Theodorsen, T., and Mutchler, W., "General theory of aerodynamic instability and the mechanism of flutter," 1935.
- [20] Wagner, H., "Über die Entstehung des dynamischen Auftriebes von Tragflügeln," ZAMM-Journal of Applied Mathematics and Mechanics/Zeitschrift für Angewandte Mathematik und Mechanik, Vol. 5, No. 1, 1925, pp. 17–35.
- [21] Küssner, H. G., "Zusammenfassender Bericht über den instationären Auftrieb von Flügeln," *Luftfahrtforschung*, Vol. 13, No. 12, 1936, pp. 410–424.
- [22] von Kármán, T., "Airfoil Theory for Non-Uniform Motion," *Journal of the Aeronautical Sciences*, Vol. 5, No. 10, 1938, pp. 379–390. https://doi.org/10.2514/8.674.

- [23] Corkery, S. J., and Babinsky, H., "An investigation into gust shear layer vorticity and the added mass force for a transverse wing-gust encounter," AIAA Scitech 2019 Forum, 2019, p. 1145.
- [24] Katz, J., and Plotkin, A., Low-speed aerodynamics, Vol. 13, Cambridge university press, 2001.
- [25] Ramesh, K., Gopalarathnam, A., Granlund, K., Ol, M. V., and Edwards, J. R., "Discrete-Vortex Method with Novel Shedding Criterion for Unsteady Aerofoil Flows with Intermittent Leading-Edge Vortex Shedding," *Journal of Fluid Mechanics*, Vol. 751, 2014, pp. 500–538. https://doi.org/10.1017/jfm.2014.297.
- [26] Sedky, G., Lagor, F. D., and Jones, A., "Unsteady aerodynamics of lift regulation during a transverse gust encounter," *Phys. Rev. Fluids*, Vol. 5, 2020, p. 074701. https://doi.org/10.1103/PhysRevFluids.5.074701, URL https://link.aps.org/doi/10.1103/PhysRevFluids.5.074701.
- [27] Goman, M., and Khrabrov, A., "State-space representation of aerodynamic characteristics of an aircraft at high angles of attack," *Journal of Aircraft*, Vol. 31, No. 5, 1994, pp. 1109–1115. https://doi.org/10.2514/3.46618, URL https://doi.org/10.2514/3.46618.
- [28] Berkooz, G., Holmes, P., and Lumley, J. L., "The proper orthogonal decomposition in the analysis of turbulent flows," *Annual review of fluid mechanics*, Vol. 25, No. 1, 1993, pp. 539–575.
- [29] Schmid, P. J., "Dynamic mode decomposition of numerical and experimental data," *Journal of fluid mechanics*, Vol. 656, 2010, pp. 5–28.
- [30] Rowley, C. W., and Dawson, S. T., "Model reduction for flow analysis and control," Annu. Rev. Fluid Mech, Vol. 49, No. 1, 2017, pp. 387–417.
- [31] Williams, M. O., Kevrekidis, I. G., and Rowley, C. W., "A Data–Driven Approximation of the Koopman Operator: Extending Dynamic Mode Decomposition," *Journal of Nonlinear Science*, Vol. 25, No. 6, 2015, pp. 1307–1346. https://doi.org/10.1007/s00332-015-9258-5.
- [32] Proctor, J. L., Brunton, S. L., and Kutz, J. N., "Dynamic mode decomposition with control," *SIAM Journal on Applied Dynamical Systems*, Vol. 15, No. 1, 2016, pp. 142–161.
- [33] Deem, E. A., Cattafesta, L. N., Hemati, M. S., Zhang, H., Rowley, C., and Mittal, R., "Adaptive separation control of a laminar boundary layer using online dynamic mode decomposition," *Journal of Fluid Mechanics*, Vol. 903, 2020.
- [34] Hjalmarsson, H., Gevers, M., Gunnarsson, S., and Lequin, O., "Iterative feedback tuning: theory and applications," *IEEE Control Systems Magazine*, Vol. 18, No. 4, 1998, pp. 26–41.
- [35] Uchiyama, M., and Mihara, M., "Determination of malonaldehyde precursor in tissues by thiobarbituric acid test," *Analytical biochemistry*, Vol. 86, No. 1, 1978, pp. 271–278.
- [36] Xu, X., Gementzopoulos, A., Girguis, S., Jones, A. R., and Lagor, F. D., "Iterative Manuever Optimization in a Transverse Gust Encounter," Conditionally accepted to AIAA Journal, ????
- [37] Brunton, S. L., and Rowley, C. W., "Empirical state-space representations for Theodorsen's lift model," *Journal of Fluids and Structures*, Vol. 38, 2013, pp. 174–186.
- [38] Xia, X., and Mohseni, K., "Unsteady aerodynamics and vortex-sheet formation of a two-dimensional airfoil," *Journal of Fluid Mechanics*, Vol. 830, 2017, pp. 439–478.
- [39] Narsipur, S., Gopalarathnam, A., and Edwards, J. R., "Low-Order Model for Prediction of Trailing-Edge Separation in Unsteady Flow," AIAA Journal, Vol. 57, No. 1, 2019, pp. 191–207. https://doi.org/10.2514/1.J057132.
- [40] Xia, X., and Mohseni, K., "Lift evaluation of a two-dimensional pitching flat plate," *Physics of Fluids*, Vol. 25, No. 9, 2013, p. 091901.
- [41] Sureshbabu, A. V., Medina, A., Rockwood, M., Bryant, M., and Gopalarathnam, A., "Theoretical and experimental investigation of an unsteady airfoil in the presence of external flow disturbances," *Journal of Fluid Mechanics*, Vol. 921, 2021. https://doi.org/10.1017/jfm.2021.484.
- [42] Xu, X., and Lagor, F. D., "Quasi-Steady Effective Angle of Attack and Its Use in Lift-Equivalent Motion Design," AIAA Journal, Vol. 0, No. 0, 2021, pp. 1–14. https://doi.org/10.2514/1.J059663, URL https://doi.org/10.2514/1.J059663.
- [43] Vatistas, G. H., Kozel, V., and Mih, W., "A simpler model for concentrated vortices," *Experiments in Fluids*, Vol. 11, No. 1, 1991, pp. 73–76.

- [44] SureshBabu, A. V., Ramesh, K., and Gopalarathnam, A., "Model reduction in discrete-vortex methods for unsteady airfoil flows," *AIAA Journal*, Vol. 57, 2019, pp. 1409–1422. https://doi.org/10.2514/1.J057458.
- [45] Hemati, M. S., Eldredge, J. D., and Speyer, J. L., "Improving vortex models via optimal control theory," *Journal of Fluids and Structures*, Vol. 49, 2014, pp. 91–111.
- [46] Bryson, A. E., and Ho, Y.-C., Applied optimal control: optimization, estimation, and control, Routledge, 1975.
- [47] Leishman, G. J., Principles of helicopter aerodynamics, Cambridge University Press, 2006.
- [48] Jones, R. T., "Operational treatment of the nonuniform-lift theory in airplane dynamics," Tech. rep., 1938.